An inverse method to interpret colour-magnitude diagrams

J.-L. Vergely[1], J. Köppen[1,2,3], D. Egret[1], and O. Bienaymé[1]

[1] Observatoire Astronomique de Strasbourg, UMR 7550, Université Louis Pasteur, Strasbourg, France
[2] Institut für Theoretische Physik und Astrophysik der Universität, D-24098 Kiel, Germany
[3] International Space University, Parc d'Innovation, F-67400 Illkirch, France

Abstract. An inverse method is developed to determine the star formation history, the age-metallicity relation, and the IMF slope from a colour-magnitude diagram. The method is applied to the Hipparcos HR diagram. We found that the thin disk of our Galaxy shows a peak of stellar formation 1.6 Gyr ago. The stars close to the Sun have a solar metallicity and a mean IMF index equal to 3.2. However, the model and the evolutionary tracks do not correctly reproduce the horizontal giant branch.

Key words. Methods: statistical – Stars: formation – Stars: luminosity function, mass function – Galaxy: formation

1. Introduction

The Hertzsprung-Russell diagram or its directly-observable counterpart, the colour-magnitude diagram (CMD) contains information about the age distribution of a stellar population, the initial mass function (IMF), and the metallicity of the stars. The distribution of the stars in such a diagram is essential for our understanding of the formation and evolution of the galaxy to which the stars belong.

In order to infer the star formation history (SFH), one usually tries to match the CMD as closely as possible by model populations computed with various scenarios for the SFH. The quality of the agreement between observed and predicted CMDs is assessed either qualitatively by visual inspection or quantitatively, e.g. by the χ^2-test (cf. Dolphin, 1997). Often, one represents the SFH by a number of discrete values or by a suitable analytic form, and adopts either a fixed metallicity or a certain age-metallicity relation. This approach, which could be called the direct or synthetic method, has been widely used (Tolstoy et al. 1993, Gallart et al. 1996, Haywood et al. 1997). Since one usually keeps the number of free parameters for the underlying model as small as necessary or practical, the adopted functional forms for the SFH and age-metallicity relation (AMR) impose certain limitations on what type of model populations are possible to be considered. Thus the obtained best fit is only optimal in the context of the adopted model, which may not necessarily represent the real galaxy. In what sense the

interpretation will be limited by these constraints is difficult to assess accurately, and can only be done by experimentation. In most recent work (Harris & Zaritsky 2001, Dolphin 2001) these limitations are being overcome by using more efficient minimization techniques. The technique of inverse methods (Craig & Brown, 1986; Tarantola & Valette, 1982a,b; Twomey, 1977) deals with such a problem in the opposite way: One tries to determine the functional form of e.g. the SFH with as much freedom as possible – with a resolution that depends on the information contained in the data – under the constraint that it matches the observed data. Such a method has been applied to the CMD by Hernandez et al. (1999): this work presents a non-parametric method for the maximum likelihood solution of the SFH, through the iterative solution of an integro-differential equation. The method presented here is similar and has the advantage of determining not only the SFH from CMD but also the IMF slope and the AMR with a temporal resolution as high as possible. Specific tools are presented in order to estimate the validity of the inverse procedure like the a posteriori covariance and the resolution. We apply our method to the Hipparcos data for solar neighbourhood stars in order to give constraints on the Galaxy thin disk formation.

2. Relation between SFH and the HR diagram

The distribution of stars in a CMD is determined by the following ingredients:

– the SFH $\psi(t)$ specifies the number of stars of all masses born as a function of age t;

- the initial mass function (IMF) gives the number N of stars in each generation per unit interval in stellar mass M. A convenient form is a power-law

$$dN \ \propto \ M^{-\Gamma} \ dM$$

where the index $\Gamma = 2.35$ refers to Salpeter's (1955) function. As usual, it is assumed to be independent of time;
- due to the chemical evolution of a galaxy, the chemical composition of the gas from which stars are born changes with time. This is described by an age-metallicity relation (AMR) $Z(t)$;
- the results of stellar evolution calculations give the properties – temperature, luminosity – of a star of given mass and metallicity for any given time after its birth;
- stellar atmosphere models give the photometric colours for any star.

For comparison with models, one bins the CMD in some suitable way in colour index and magnitude. Then the number density of stars in a given bin q can be written as

$$D_q = \int \psi(t) F_q(t, Z(t), \Gamma) dt \tag{1}$$

the superposition of the contributions from all stellar populations of single age t, metallicity Z, and IMF slope Γ. Since the densities $F_q(t, Z, \Gamma)$ would be computed from stellar evolutionary tracks and the photometric colours, the interpretation of the observations $D_q = D_q(\text{obs})$ consists in solving Eqn. 1 for the SFH ψ.

In principle, one would like to determine all three functions SFH, IMF, and AMR, i.e. functions defined on an infinite number of points. However huge the observed set of data might be, it remains finite. Thus, even if there were no noise and observational uncertainties, one can derive the three functions only up to a certain limit of detail.

The usual approach is to assume that the functions have some specified analytical form described by a few parameters – such as the exponent in the power-law for the IMF, or a simple SFH with a few rectangular starbursts – and the objective is simply to find the best model of this type that reproduces the observations. In doing so, one does not know of what (time) resolution could be reached with the data available, and thus one may not make full use of what the observations could furnish.

3. The inverse method

The determination of the full functional form of the SFH (or AMR or IMF) from a CMD is an under-determined problem, because the amount of observational data is only finite and thus cannot provide the information for every detail of the function. Application of a straight inversion technique to Eqn. 1 could be very sensitive to the noise in the data, and could well give mathematically correct but unphysical results (Craig & Brown 1986). The problem can be regularized by demanding that the true solution is smooth in some suitably quantified sense (Twomey 1977, Craig & Brown 1986). Thus one reduces the number of free parameters, and the problem becomes well-posed.

Tarantola & Valette (1982a) use a Bayesian approach which describes how the a priori knowledge about the functions – which might be the null information – is changed by the information contained in the observational data. If the data contain no information about a parameter, one would merely retrieve its a priori value. The a posteriori probability density $f_{\text{post}}(M|D)$ for the vector M containing the unknown model parameters, given the observed data D, is linked by Bayes' theorem

$$f_{\text{post}}(M|D) \propto L(D|M) \cdot f_{\text{prior}}(M)$$

to the likelihood function L and the prior density function for the parameter vector. The factor of proportionality is obtained by normalization $\int f_{\text{post}}(M|D) dM = 1$ over all parameter space.

The theoretical model shall be described by an operator g which connects the model parameters M with the predicted data

$$D_{\text{predicted}} = g(M)$$

which is to agree as closely as possible with the observed data. If we assume that both the prior probability and the errors in the data are distributed as Gaussian functions, the posterior distribution becomes

$$f_{\text{post}}(M|D) \ \propto \ \exp(-\frac{1}{2}(D - g(M))^T C_D^{-1}(D - g(M))$$
$$-\frac{1}{2}(M - M(0))^T C_0^{-1}(M - M(0)))$$

The prior is specified by the value $M(0)$ of the parameter vector and its variance-covariance matrix C_0. The matrix C_D specifies how the variances in the observed data are obtained (e.g. if a non-Gaussian distribution of the observational errors is to be approximated) and whether one needs to take into account correlations between the individual data.

In this method the model parameters may include single value parameters as well as entire functions. For simple parameters, C_0 is the matrix of its a priori variances and a priori covariances between each parameter. The variances and covariances would be chosen to be large, if we do not have any initial knowledge about the parameter values. On the other hand, if the values are accurately known, one would use variances correspondingly smaller. For a function, C_0 is a functional operator which has for its kernel the auto-correlation function. Most commonly one uses a Gaussian kernel:

$$C_0(x, x') = \sigma_0(x)\sigma_0(x') \exp\left(-\frac{(x - x')^2}{\xi_0^2}\right)$$

$\sigma_0(x)$ – which can be any function of x – describes how strongly the solution is allowed to fluctuate between points, and ξ_0 is the smoothing length for the solution.

Other types of kernels may be employed, e.g. an exponential kernel which would smooth the solution differently.

The best estimator $\tilde{M}$ for M is the most probable value of M, knowing the set of data D. This condition is reached by minimizing the quantity

$$\frac{1}{2}(D - g(M))^T C_D^{-1}(D - g(M))$$
$$+\frac{1}{2}(M - M(0))^T C_0^{-1}(M - M(0)) \qquad (2)$$

which corresponds to a maximum likelihood condition.

Since the operator g is non-linear, the solution for the parameter vector must be done iteratively (Tarantola & Valette 1982a, 1982b):

$$\tilde{M}(k+1) = M(0) + C_0 G^T(k)(C_D + G(k)C_0 G^T(k))^{-1}$$
$$(D + G(k)[\tilde{M}(k) - M(0)] - g(\tilde{M}(k))) \quad (3)$$

with k counting the number of iterations, and the matrix of partial derivatives

$$G(k) = \frac{\partial g(M(k))}{\partial M}$$

For use in subsequent equations we shall abbreviate:

$$S := C_D + G(k) \cdot C_0 \cdot G^T(k)$$

3.1. Formulation of the problem

The CMD is binned both in M_V and (B–V), by dividing the range of interest of M_V–values into m intervals of equal length ΔM_V. Likewise, the range of (B–V) values is divided into n intervals of equal length Δ(B–V). Then, $D(i, j)$ is the number of stars having their magnitude M_V between M_{V_i} and $M_{V_i} + \Delta M_V$ as well as their colour index (B–V) between $(B–V)_j$ and $(B–V)_j + \Delta$(B–V). For a less cumbersome notation, we use a single index $q = (i - 1)n + j = 1 \ldots nm$ corresponding to bin (i, j).

Synthetically-generated stellar populations for single ages t, metallicities Z, and IMF slopes Γ are used to specify which fraction of the total number of stars is found in each bin q

$$F_q(t, Z, \Gamma) \, \Delta M_V \, \Delta(B–V) \qquad (4)$$

Convolving these populations with the SFH by Eqn. 1 gives the number density D_s of stars in that bin.

Since the star formation rate is always positive, changing over from ψ to $\alpha(t)$

$$\alpha(t) := \ln(\psi(t)/\psi_0) \qquad (5)$$

where ψ_0 is a constant, will enforce this physical fact. We shall assume that the uncertainties in the function $\alpha(t)$ follow a Gaussian law. This implies that the errors in $\psi(t)$ follow a log-normal distribution.

Since the position of isochrones in the CMD is a nearly logarithmic function of the age, it is more appropriate to use $u := \lg(t)$ instead of the linear age t. With $dt =$

$10^u \ln(10) \, du$ and the abbreviation $h(u) := 10^u \ln(10)$, Eqn. 1 is written as

$$D_q = \int \psi_0 \exp(\alpha(u)) F_q(u, Z(u), \Gamma) h(u) du$$
$$=: g_q(M) \qquad (6)$$

This defines g_q as a non-linear operator acting on the parameter vector M which consists of the unknown functions $\alpha(t)$ and $Z(t)$, and the unknown parameter Γ:

$$M = \begin{pmatrix} \alpha(t) \\ Z(t) \\ \Gamma \end{pmatrix}$$

We note in passing that the IMF could of course also be taken as an unknown function $\phi(m)$. This would merely increase greatly the dimension of parameter space, resulting for the numerical solution of the equations in greater memory requirements and unacceptable execution times. Furthermore, an arbitrary IMF would be largely degenerate with the SFR, at least on the main sequence.

3.2. The base models

The operator g_q (Eqn. 6) generates the model CMDs from a set of base models $F_q(u, Z, \Gamma)$ (Eqn. 4) by integrating over all ages. The base models are computed from synthetic stellar populations of a single age t, metallicity Z, and specified IMF; they give the probability of finding a star in bin q in the CMD, depending on the model parameters, but we also take into account observational selection effects:

– synthetic theoretical stellar populations are computed from the isochrones of Bertelli et al. (1994) which directly give the positions in the $(M_V, (B–V))$–diagram for stars in the mass range 0.6 to 120 $M_\odot$;
– the IMF is a power-law between the stellar mass limits of 0.6 and 80 $M_\odot$;
– the stars are uniformly and randomly distributed in space;
– the limiting magnitude is 8.0 mag in V band.

A grid of models was computed, each comprising 2 million stars (before applying selections), for any combination among 50 ages distributed linearly between $u = 6.6$ and 10.3, 10 metallicities between $Z = 0.0004$ and 0.05, and 5 IMF slopes between 2.0 and 4.5. This was done through linear interpolation in age and metallicity from the Padua isochrones.

All integrals are evaluated numerically, with the rectangle method being sufficiently accurate.

4. Determination of SFH and IMF slope

We shall first consider the case of deducing simultaneously the SFH and the slope of the IMF: The parameter vector

M consists of the unknown function $\alpha(t)$ and the unknown parameter Γ:

$$M = \begin{pmatrix} \alpha(t) \\ \Gamma \end{pmatrix}$$

The metallicity is considered to be known and constant.

Then, the matrix of partial derivatives is

$$G(k) = \begin{pmatrix} \frac{\partial g_1}{\partial \alpha} & \frac{\partial g_1}{\partial \Gamma} \\ \frac{\partial g_2}{\partial \alpha} & \frac{\partial g_2}{\partial \Gamma} \\ \vdots & \vdots \\ \frac{\partial g_s}{\partial \alpha} & \frac{\partial g_s}{\partial \Gamma} \end{pmatrix}$$

with $s = nm$ the total number of data bins.

Equation 3 gives the procedure to improve an estimate of the parameters. For better legibility, we drop the dependence on the iteration number k of G, $\alpha(u)$, and Γ. The (i,j)-th component of the matrix product is (for all $i, j = 1, \ldots s$)

$$
\begin{aligned}
(GC_0G^T)_{i,j} &= \int\int C_\alpha(u,u')\psi_0^2 \exp(\alpha(u) + \alpha(u')) \\
&\quad \times F_i(u,\Gamma)F_j(u',\Gamma)h(u)h(u')dudu' \\
&\quad + \left(\int \psi_0 \exp(\alpha(u)) \frac{\partial F_i(u,\Gamma)}{\partial \Gamma} h(u)du \right) \\
&\quad \times \sigma_\Gamma^2 \left(\int \psi_0 \exp(\alpha(u)) \frac{\partial F_j(u,\Gamma)}{\partial \Gamma} h(u)du \right)
\end{aligned}
$$

The variance-covariance matrix C_0 of the prior distribution of the parameters is

$$C_0 = \begin{pmatrix} C_\alpha & 0 \\ 0 & \sigma_\Gamma^2 \end{pmatrix}$$

and the covariance function C_α

$$C_\alpha(u,u') = \sigma_\alpha^2 \exp\left(-\frac{(u-u')^2}{\xi_\alpha^2} \right) \tag{7}$$

with ξ_α the correlation length in $\lg(t)$.

The i-th component of the vector $V(k) = D - g(M) + G(k)(M - M(0))$, which depends on the iteration index k, is computed from

$$
\begin{aligned}
V_i = D_i &\quad + \int \psi_0 \exp(\alpha(u))(\alpha(u) - 1)F_i(u,\Gamma)h(u)du \\
&\quad + \int \psi_0 \exp(\alpha(u))(\Gamma - \Gamma_0) \frac{\partial F_i(u,\Gamma)}{\partial \Gamma} h(u)du
\end{aligned}
$$

Defining the vector $W(k) = S^{-1}V(k)$, the $k+1$-st estimate for the parameters is computed from their k-th values by

$$
\begin{aligned}
\alpha_{k+1}(u) = \sum_i W_i(k) &\quad \int C_\alpha(u,u')\psi_0 \exp(\alpha_k(u')) \\
&\quad \times F_i(u',\Gamma_k)h(u')du'
\end{aligned}
$$

and

$$
\begin{aligned}
\Gamma_{k+1} = \Gamma_0 + \sum_i W_i(k)\sigma_\Gamma^2 &\quad \int \psi_0 \exp(\alpha_k(u')) \\
&\quad \times \frac{\partial F_i(u',\Gamma_k)}{\partial \Gamma} h(u')du'
\end{aligned}
$$

The estimator for ψ from α is given by the relation (e.g. Saporta, 1990):

$$\tilde{\psi}(u) = \psi_0 \exp\left(\alpha(u) + \frac{\sigma_{\alpha(u)}^2}{2} \right)$$

with the dispersion of the posterior distribution for $\alpha(t)$

$$\sigma_{\psi(u)} = \psi_0 \sqrt{\exp(2\alpha(u) + \sigma_{\alpha(u)}^2)\left(\exp(\sigma_{\alpha(u)}^2) - 1\right)}$$

where $\sigma_{\alpha(u)}$ is the dispersion of the posterior distribution of α (Eqn. 9 below).

In the computations, the derivatives such as the matrix G and $\partial F/\partial \Gamma$ are evaluated numerically. The functions $\partial F/\partial \Gamma$ are interpolated by a 4 th order polynomial.

4.1. The posterior variance-covariance matrix

The internal errors made by the method on the estimated parameter values can approximately be computed. This is done by a second-order expansion of the posterior density distribution in the neighbourhood of the best solution:

$$C_{\tilde{M}} = C_0 - C_0 G^T S^{-1} G C_0 \tag{8}$$

For the simple parameter of the IMF slope one gets

$$\sigma_{\tilde{\Gamma}} = \sigma_\Gamma \sqrt{(1 - G^T S^{-1} G)},$$

and for the function $\alpha(u)$:

$$\sigma_{\alpha(u)} = \sqrt{\sigma_\alpha^2 - C_\alpha G^T S^{-1} G C_\alpha}. \tag{9}$$

4.2. Resolving kernel and mean index

Observational errors, like the finite photometric accuracy, will degrade the information contained in the CMD, and thus cause an additional loss of resolution in age. The concept of the resolving kernel, introduced by Backus & Gilbert (1970), permits us to compute how much a stellar population for a given age is spread out in age. Suppose that we knew the true model M_{true}, then the observed data would be

$$D = g(M_{\text{true}}).$$

If the operator g were linear, so that $G_k = G = g$, then Eqn. 3 shows how the deviation of the true model parameters from the initial guess is expected to be degraded into the observed one

$$\tilde{M} - M_0 = C_0 G^* S^{-1} G(M_{\text{true}} - M_0). \tag{10}$$

The operator – called the resolving kernel –

$$K(u,u') := C_0 G^* S^{-1} G$$

describes this degradation of information. Though it applies strictly for linear models only, it remains a good approximation in our problem as well: the density of stars in a bin is a linear function of the SFH. Because the values

for the SFH remain within a factor of 10 or so, the logarithmic relation with the parameter α does not represent a strong non-linearity.

The relation between the resolving kernel K and the a posteriori variance-covariance operator $C_{\tilde{M}}$ is computed as follows from Eqn. 8:

$$C_{\tilde{M}} = (I - C_0 G^T S^{-1} G) C_0 = (I - K) C_0$$

this yields:

$$K = I - C_{\tilde{M}} C_0^{-1}$$

I is the Dirac function if the unknown parameter is a function (the SFH in our case). So, if the posterior variance-covariance operator increases, the amplitude of the resolving kernel decreases and the width increases.

Another important and useful concept is a measure of the information present in the data. This is closely linked to the resolving kernel: Suppose that the mean value of the SFH is within the width of the kernel K, so Eqn. 10 gives

$$(\tilde{M} - M(0))(u) = (M_{\text{true}} - M(0))_{\text{mean}} \cdot \int K(u, u') du'.$$

The integral is called the *mean index* $I(u)$

$$I(u) := \int K(u, u') du'$$

which has the following meaning: If $I(u)$ has very low values, the expected model would be close to the initial guess, irrespective of how much the initial model would differ from the true model. The quality of the SFH estimator thus is poor. But if $I(u) \approx 1$ the deduced model would be close to the true model.

We note that if we take an a priori variance-covariance operator with too large a smoothing length ξ_α, we will obtain a good mean index. However, the a posteriori resolution will be poor.

5. Simultaneous derivation of SFH and AMR

We now address the problem of determining simultaneously two functions, the SFH and the AMR. The parameter vector is

$$M = \begin{pmatrix} \alpha(t) \\ Z(t) \end{pmatrix}.$$

The variance-covariance matrix of the parameter priors is taken as:

$$C_0 = \begin{pmatrix} C_\alpha & 0 \\ 0 & C_Z \end{pmatrix}$$

i.e. we assume that SFH and AMR are a priori uncorrelated. This is done for simplicity. We note that chemical evolution of the galaxy would impose a strong relation between the two functions and could be used to compute such a correlation.

C_α is given by Eqn. 7, and C_Z is given by

$$C_Z(u, u') = \sigma_Z^2 \exp\left(-\frac{(u - u')^2}{\xi_Z^2}\right).$$

The derivation is nearly identical as before, with $\alpha(u)$ and $Z(u)$ depending on the iteration index k:

$$(GC_0 G^*)_{i,j} = \int\int C_\alpha(u, u') \psi_0^2 \exp(\alpha(u) + \alpha(u'))$$
$$\times F_i(u, Z(u)) F_j(u', Z(u')) h(u) h(u') du du'$$
$$+ \int\int C_Z(u, u') \psi_0^2 \exp(Z(u) + Z(u'))$$
$$\times \frac{\partial F_i(u, Z(u))}{\partial Z} \frac{\partial F_j(u', Z(u'))}{\partial Z} h(u) h(u') du du'$$

In addition to the iteration for the SFH which proceeds as before, we have for the AMR

$$Z_{k+1}(u) = Z_0(u) + \sum_i W_i(k) \int C_Z(u, u') \psi_0 \exp(Z_k(u'))$$
$$\times F_i(u', Z_k(u')) h(u') du'$$

where $Z_0(t)$ is the a priori age-metallicity-relation.

6. Validation of the method by simulations.

In practice, the large amount of computing time necessary makes it prohibitive to determine simultaneously the SFH, AMR, and the IMF slope. Therefore, in the following tests we show an inversion of SFH and IMF slope only. Also, to limit the number of bins and hence the computing time, we consider only the histogram of the (B–V)– colour index. The colour of the turn-off is very sensitive to the age of a stellar population, thus one obtains a good resolution of the SFH. The range from −0.3 to 1.7 is divided into bins of 0.02 mag width, the observational error. It is not useful to use cell sizes smaller than this error.

The variance-covariance matrix C_D for the data is assumed to be diagonal, as we shall assume that there are no correlation between the numbers of stars in different bins. To approximate the Poisson noise in the stellar numbers, we take the variance equal to the number of stars in a bin.

Since our method is an iterative procedure, it yields models that approach the data successively closer with each step. The distance between model prediction and observed data can be measured by the value of χ^2:

$$\chi^2 = \sum_s \frac{(g_s(M) - D_s)^2}{D_s}$$

The convergence is usually monotonic. Typically 10 iterations suffice to achieve a value of χ^2 stable within 10^{-2} for the determination of the SFH.

In our formalism, the errors in the data are assumed to be normally distributed. This is an approximation valid only if each bin contains a large number of stars, whereas in reality the errors in the histogram are distributed with a Poisson law.

As simulated observational data we took a stellar population model having a fixed (solar) metallicity, a power-law IMF with slope 2.25, and a star formation history involving several bursts at different ages and with different

strengths (shown as the full line in the middle left panel of Fig. 1).

We have to specify the parameter σ_α which quantifies how large a fluctuation we accept in the SFH. We chose it in such a way that one obtains reduced $\chi^2 = 0.5...1.5$. Smaller values would show that the data are over-interpreted, but larger values indicate that the model reproduces the observations only poorly. It turns out that $\sigma_\alpha = 1$ is a good choice. The value of the smoothing length ξ_α is normalised as $\sigma_\alpha^2 \simeq cste/\xi_\alpha$.

In Fig. 1 we show the results obtained for the data to which Gaussian noise had been added with an amplitude of $\sigma_{M_V} = 0.3$ mag and $\sigma_{(B-V)} = 0.01$ mag. The best solution has a reduced $\chi^2 = 0.77$, and as the top panels show, the stellar population is closely reproduced. The slope of the IMF is $\Gamma = 2.16 \pm 0.08$, i.e. slightly flatter than had been assumed. The middle panels depict that the deduced SFH well matches all the features of the assumed SFH older than about 100 Myrs. One notes that even the small SFH feature near 1 Gyr is reproduced. However, the young populations are not very well represented because the number of corresponding 'observed' stars is rather small (< 100) and, in addition, the $B - V$ colour of the main sequence becomes insensitive to age for young ages. This is also evident in the bottom panels: while the resolving kernel shows that the relative resolution in age is rather good and nearly the same for ages larger than 100 Myrs, the resolution (in $\lg t$) deteriorates for younger populations. Finally, the level of information in the CMD – as measured by the mean index – drops below about 10 Myrs.

Figure 2 presents the results for the same 'observations', but degraded with larger values $\sigma_{M_V} = 0.5$ mag and $\sigma_{(B-V)} = 0.05$ mag, which is evident from the CMDs. The reduced χ^2 obtained here is 0.64. As before, the IMF comes out somewhat too flat with $\Gamma = 1.99 \pm 0.12$. The increased noise level in the data destroys all the information about the details of the SFH for ages up to about 1 Gyr; only the oldest starbursts can be detected. The time resolution of the method has become much worse than Fig. 1 for all ages except around 1 Gyr; the drop of the mean index now occurs at about 30 Myrs.

Figure 3 presents the results of the SFH and AMR inversion from a simulated CMD composed of an old metal-poor population ($Z = 0.004$) and a young metal-rich one ($Z = 0.02$). Because the zero age main sequences are shifted with metallicity, the SFH-AMR information is not degenerated in the colour-magnitude diagram. The prior taken for the inverse process is $\psi_0 = 1$, $\alpha(t) = 0$ and $Z(t) = 0.01$, implying constant SFH and AMR. The convergence occurs after about 20 iterations.

These test results demonstrate that the method is capable of deducing reliably the history of star formation in rather fine detail. It also permits one to assess quantitatively the time resolution that is possible with a given observational data set, as well as the information it contains.

7. The local CMD from Hipparcos data

Hipparcos gives astrometry and photometry for stars within about 1 kpc of the Sun. Most of these stars belong to the thin disk, only about 5 % of them being members of the thick disk and halo (Robin et al., 1996). This sample gives us valuable information about the evolution of the thin disk of our Galaxy. This is not limited to the solar neighbourhood proper, but pertains also to a larger portion of the disk: because of the radial diffusion of stars in the disk (Wielen, 1977), one finds presently, near to the Sun, stars of different metallicities and ages.

7.1. The Hipparcos data

We have selected a sample of 13520 stars from the Hipparcos catalogue (Perryman et al.; ESA 1997) which meet these criteria:

- single stars
- the apparent magnitude limit V depends on the latitude b :

$$V \le 7.3 + 1.1|\sin(b)|$$

  for all spectral types;
- observed parallaxes should be larger than 5 mas.

Double stars may cause some problem: confirmed double stars in the Hipparcos catalogue comprise about 20% of all stars. Also, it is well known that among a stellar population about 50 % are double stars. Hence, we underestimate the presence of double stars, which could cause a bias in the following way: binaries will appear to be located on the red side of the main sequence. They will be interpreted by the model as being either of higher metallicity or in a more evolved state. Thus, the derived populations could be too old or too metal-rich.

The choice of the bin sizes is determined by the observational uncertainties of the data: For the error on the parallaxes π we take a constant value as a reasonable approximation $\sigma_\pi = 1(\text{mas})$. This results in an uncertainty of the absolute magnitudes of $\sigma_{M_V} = 2.17\sigma_\pi/\pi$ which reaches 0.5 mag at 200 pc. The error in the colour (B–V) is taken as constant at 0.02 (mean error in the Hipparcos catalog). Therefore, we divide the HR diagram into cells of 0.5 mag in M_V and 0.02 in (B–V). To prevent nearly empty cells with their large relative fluctuations of occupation numbers to influence the results too strongly, we increase the cell size, if necessary, so that each bin shall contain at least 5 stars. The resulting cell layout is presented in Fig. 5.

With the limit on apparent magnitude and the local density of the stars, one expects only very few stars below 0.6 $M_\odot$. Thus, the isochrones of Bertelli et al. (1994) which pertain only to stars above 0.6 $M_\odot$ are entirely adequate.

Absolute magnitudes and colour indices are corrected for interstellar extinction with the model of Vergely (1998) which gives the opacity at each point of the space in the 250 pc sphere surrounding the Sun, derived with a tomographic technique from Hipparcos data and Strömgren photometry.
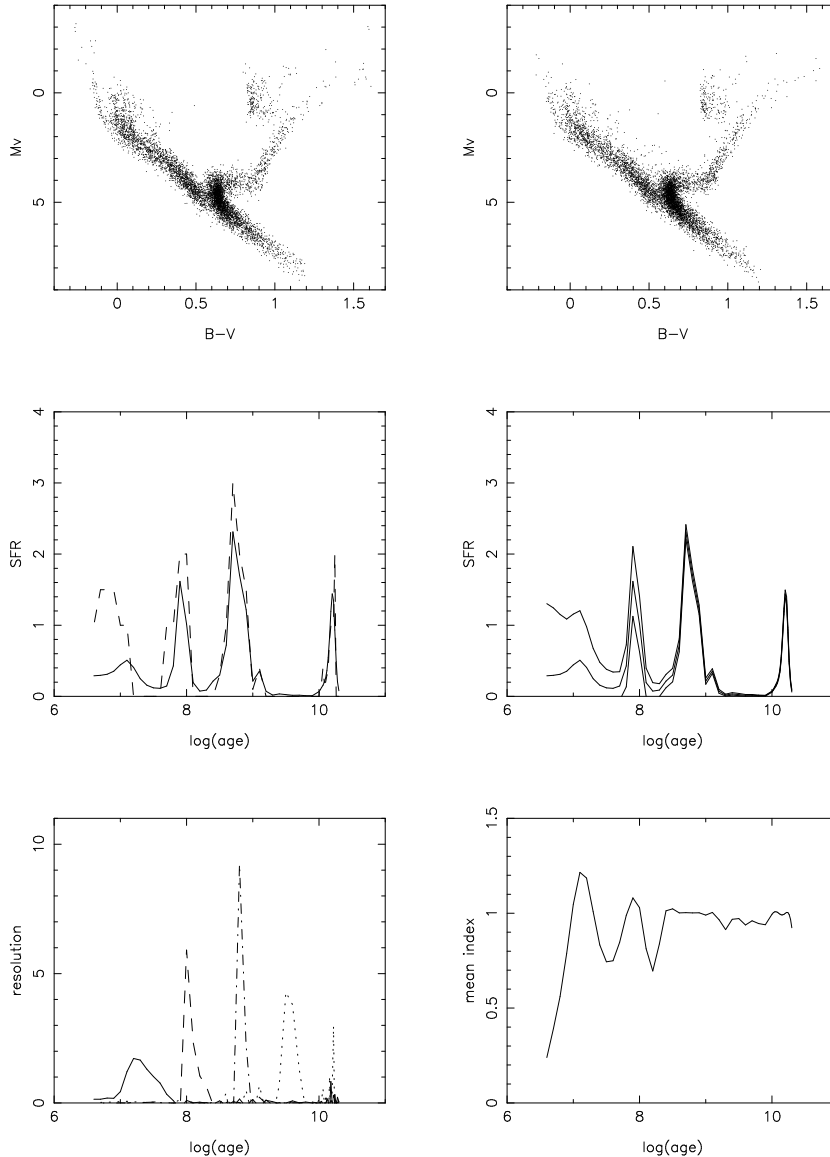
Fig. 1. The top panels show the simulated 'observed' CMD (left) with $\sigma_{M_V} = 0.3$ and $\sigma_{(B-V)} = 0.01$ and the best model (right). The middle left panel shows the assumed SFH (dashes) and the best model (full line), on the right is the best model at $\pm 1\sigma$. The bottom left panel shows the resolving kernel $K(t, t')$ as a function of age t for $\log(t') = 7.3$, 8.1, 8.8, and 9.6 (full, dashes, dot-dashes, and dots), and at right the mean index. Note that the fit for the tests is performed on the $B - V$ distribution only, not on the full 2-D CMD distribution.

7.2. The base models $F(u)$

The construction of the base models follows that described in Sect. 3.2, but we now take into account the above-mentioned selection criteria for the observational data.

Furthermore, for solar neighbourhood stars, we must also take into account that older stars are distributed up to greater heights above the Galactic plane than younger ones, because the amplitude of their oscillatory motions perpendicular to the plane increases with age (cf. Wielen 1977).

In this study, we restrict our SFH-AMR analysis to the thin disk stars. The contamination by thick disk population stars can be neglected in a first approach, because

only about 5% of stars belong to the thick disk in the Hipparcos sample. The age-dispersion relation given by Gomez et al. (1997) is valid only for thin disk population stars and shows clearly that there is no significant dynamic evolution of the thin disk, after 4-5 Gyr. More accurately, the age-dispersion relation is given for old thin disk stars with age < 9 Gyr and saturated at 15-17 km/s.

The relation between age t ([Gyr]) and dispersion of the vertical velocity component W ([km/s]) has recently been derived from Hipparcos data (Gómez et al., 1997):

$$\sigma_W(t) = 17.0 - 12.0 \exp(-t/2)$$

Assuming isothermality, the density of coeval stars of age t is constrained by the vertical potential $\phi(z)$ at height z
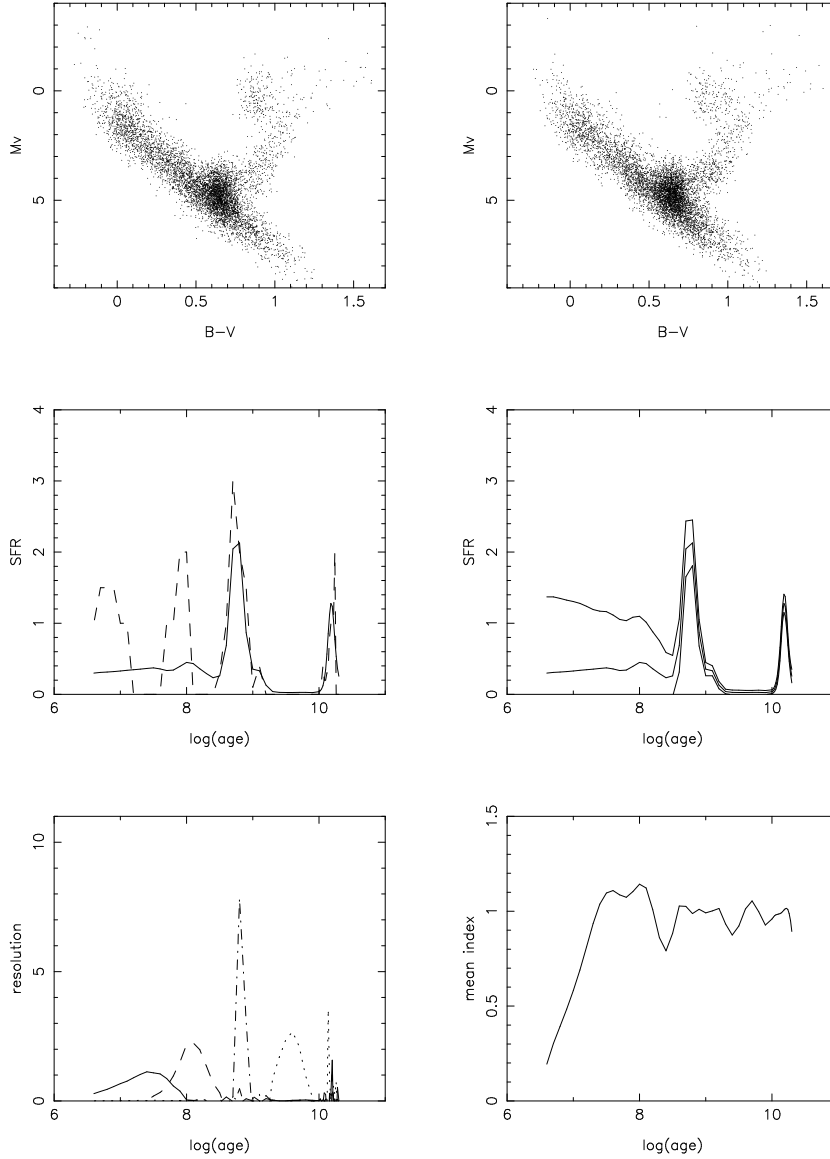
Fig. 2. Same as Fig. 1, but with $\sigma_{M_V} = 0.5$ and $\sigma_{(B-V)} = 0.05$

as:

$$\rho(t, z) = \rho(t, 0) \exp\left(-\frac{\phi(z)}{\sigma_W^2(t)}\right)$$

where $\rho(t, 0)$ is the density at $z = 0$ and $\phi(z)$ is the potential.

Recent determinations of the total local mass density ρ_0, based on Hipparcos data, give ρ_0 from 0.076 $M_\odot pc^{-3}$ (Crézé et al, 1997,1998) to 0.10 $M_\odot pc^{-3}$ (Holmberg & Flynn, 2000). The surface mass density is determined from measurements of the force at larger distances (0.5 to 1 kpc) from the galactic plane: recent determinations of Σ_0 range from 48 to 56 $M_\odot pc^{-2}$, (Kuijken & Gilmore 1989, Flynn & Fuchs 1994). These two independent sets of constraints on the vertical potential may be combined in a single formula:

$$\Phi(z) = 0.027 \, \Sigma_0(\sqrt{z^2 + D^2} - D + \rho_{eff} \, z^2) \tag{11}$$

Here, we will use the coefficients $D = 240$ pc, $\Sigma_0 = 48 M_\odot pc^{-2}$ and $\rho_{eff} = 0.0105 \, M_\odot pc^{-3}$, this implies a local mass density of 0.081 $M_\odot pc^{-3}$ and a disc surface mass density of 48 $M_\odot pc^{-2}$.

7.3. Determination of IMF slope and SFH

We first consider the metallicity to be constant, at solar value $Z = 0.02$. The resultant fit is not good (reduced $\chi^2 = 4.9$), so that the model is to be rejected.

The derived IMF slope is $\Gamma = 3.2 \pm 0.1$, steeper than Salpeter's, but quite close to the slope of 2.7 found by e.g. Kroupa, Tout & Gilmore (1993) in the solar neighbourhood for stars above 1 $M_\odot$. It is these stars that contribute to most of the data in our sample.

Main sequence magnitudes lie between about 6 and -2 mag, corresponding to masses between 0.6 and 8 $M_\odot$,
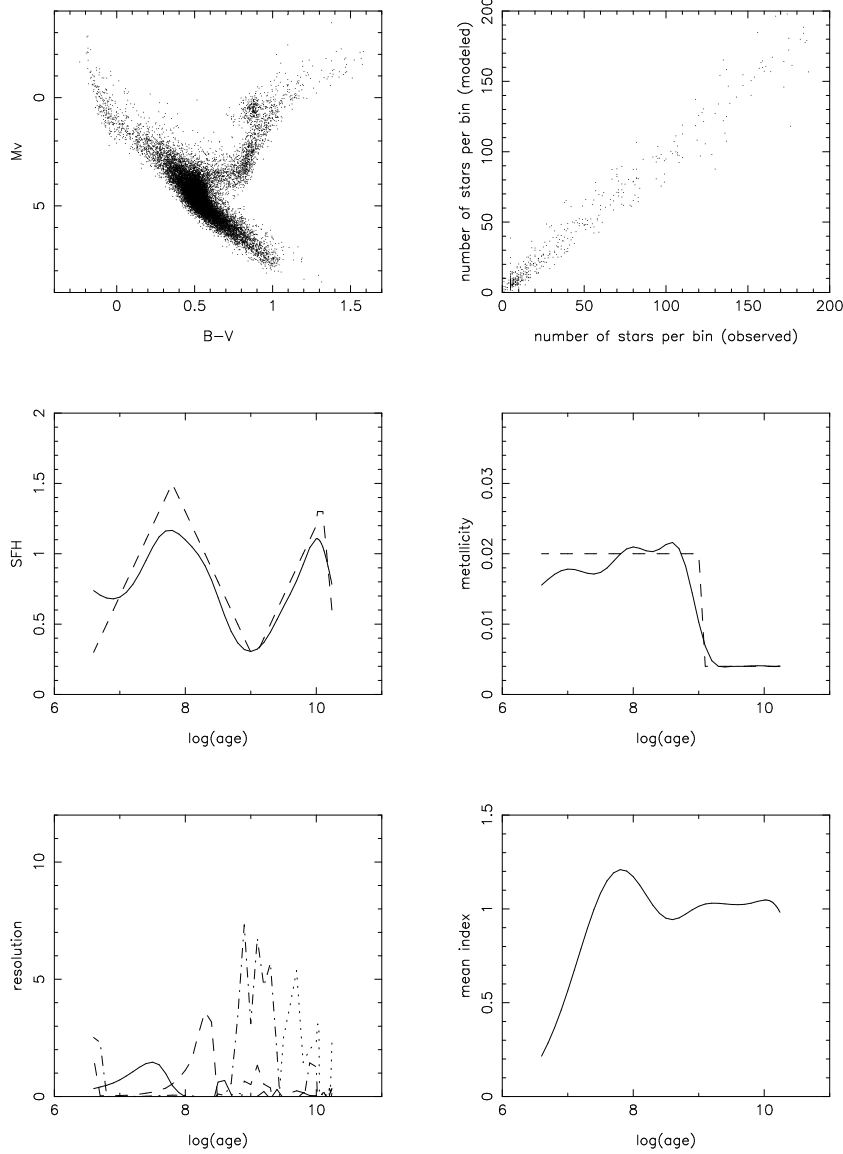
Fig. 3. The top panels show the simulated 'observed' CMD (left) with $\sigma_{M_V} = 0.3$ and $\sigma_{(B-V)} = 0.01$ and the data fitting in number of stars per bin (right). The middle left panel shows the assumed SFH (dashes) and the best model (full line); on the right is the assumed AMR (dashes) and the best model (full line). The bottom left panel shows the resolving kernel $K(t, t')$ as a function of age t for $\log(t') = 7.3$, 8.1, 8.8, and 9.6 (full, dashes, dot-dashes, and dots), and at right the mean index

and lifetimes of greater than 40 Myrs. Thus, information about the last 40 Myrs is not present. This is seen in the turn-down of the mean index (cf. Fig. 6). The prior taken for the inverse process is (see Eqn. 5) $\alpha(t) = 0$, implying a constant SFH.

The deduced SFH is presented in Fig. 6. The resolution is rather poor; from the widths of the kernels one gets 0.4 dex in the relative age. The a posteriori error is quite large for the youngest populations and the results are not significant for ages below 30 Myrs, as clearly shown by the low mean index which drops at about 50 Myrs.

7.4. Simultaneous determination of SFH and AMR

As the model with constant metallicity has to be rejected, we now investigate models with a fixed IMF slope of $\Gamma = 3.0$, but leaving both the SFH and AMR as free parameters. As priors for the inverse process we take $\alpha(t) = 0$ and $Z(t) = 0.02$, i.e. constant SFH and AMR.

If we assign equal weights to main sequence and giant stars, we obtain a rather poor value of reduced $\chi^2 = 3.7$. The model population does not fit the main sequence, in particular below it, many metal-poor stars are predicted. The reason is that the prominent red clump – composed of horizontal branch stars of nearly solar metallicity – contains many relatively blue stars which in the context of the
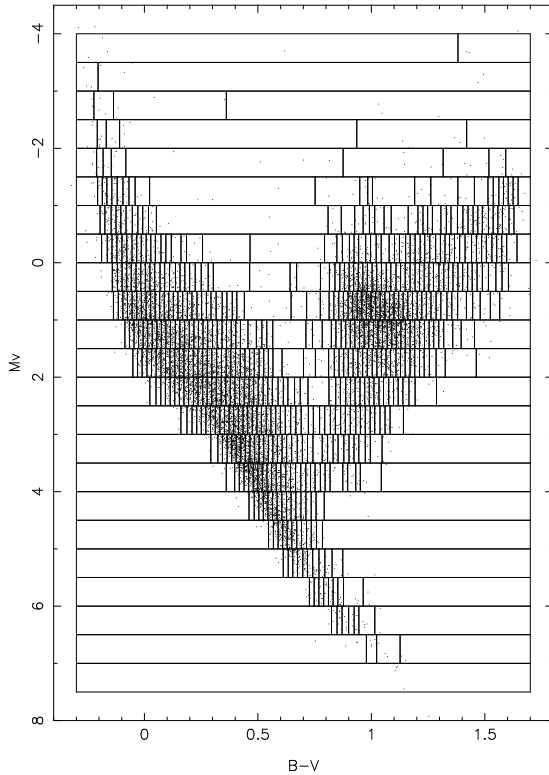
Fig. 4. The colour-magnitude diagram of the single stars of the Hipparcos catalogue, with the adopted binning in both dimensions
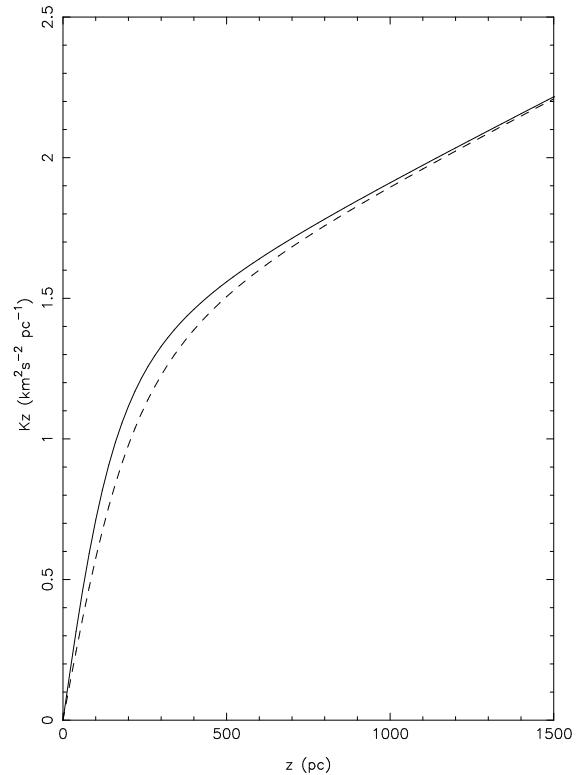

Fig. 5. The vertical potential (continuous line) force given by Kuijken & Gilmore (1989) and the modified force (dashed line) used here in order to include the most recent determinations of a local mass density in the solar neighbourhood.

presently-used stellar tracks correspond to low metallicity isochrones.

If we reduce the weight for the giants by a factor of two, a rather satisfactory fit with reduced $\chi^2 = 1.9$ is obtained. Figure 8 shows that the main sequence is well reproduced except for the odd bin, but that a major discrepancy remains with the red clump where the observed stars tend to be systematically bluer than the model. Very recently, Girardi et al. (2000) published updated isochrones. Detailed comparison with the isochrones of Bertelli et al. (1994) reveals that the horizontal branch is shifted to the blue by about 0.05 mag in (B–V) which is the right amount to remove the discrepancy (as shown by test calculations).

However, this shift could be explained by a dispersion in the AMR (not taken into account in this study) or the presence of unresolved giant binary stars.

7.4.1. The star formation history

The SFHs obtained from the two approaches are quite similar, having a rather broad peak near an age of 1.6 Gyr. The SFH at the present time deduced with the constant metallicity model is rather low, while in the model with variable metallicity (Fig. 7) it is almost as high as this peak. Note howeverthat the information available allows a reliable deduction of the SFH with good resolution only for ages larger than about 100 Myrs. The age resolution achieved in the second model is somewhat poorer, due to

the information now being used to derive the AMR as well.

A first preliminary analysis of the Hipparcos CMD by Bertelli et al. (1997) yielded that star formation occurs between ages of 0.1 and 10 Gyrs, with indication of a discontinuity at about 1.5 Gyr. Also, the broad red clump indicated a spread in metallicity. From a rather qualitative comparison they find that the SFH should have been constant or increasing from 10 to 1.5 Gyrs, and be reduced by a factor 2 or 3 after that time. Our results fully confirm these findings, showing a broad and rather well-defined peak of star formation activity at about 1.5 Gyrs with the SFH being substantially lower before and after.

Bertelli and Nasi (2000) use a comparable set of Hipparcos stars to analyse the SFH in the solar neighborhood. Their principal conclusion is that the SFH increases, in a broad sense, from the beginning to the present time; that is in agreement with the SFH obtained in this paper. They have tested different IMF slopes and preferred the IMF Salpeter slope in order to fit the main sequence. However they underline that an IMF slope of 3.35 is an acceptable solution, particulary to find the best ratio between the number of stars in the He burning phase and that in the main sequence phase. Our analysis shows that this IMF slope can fit very well the main sequence, too.
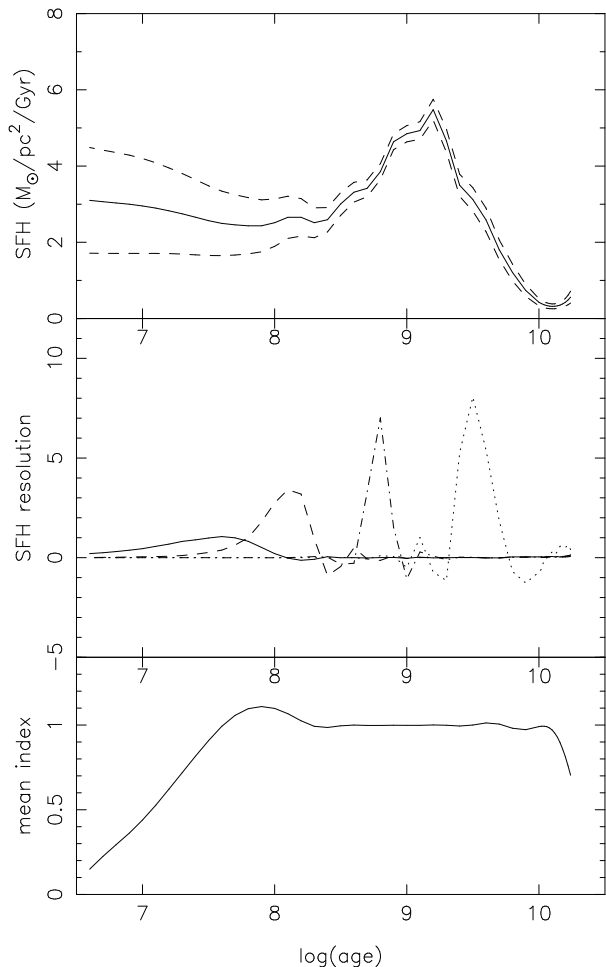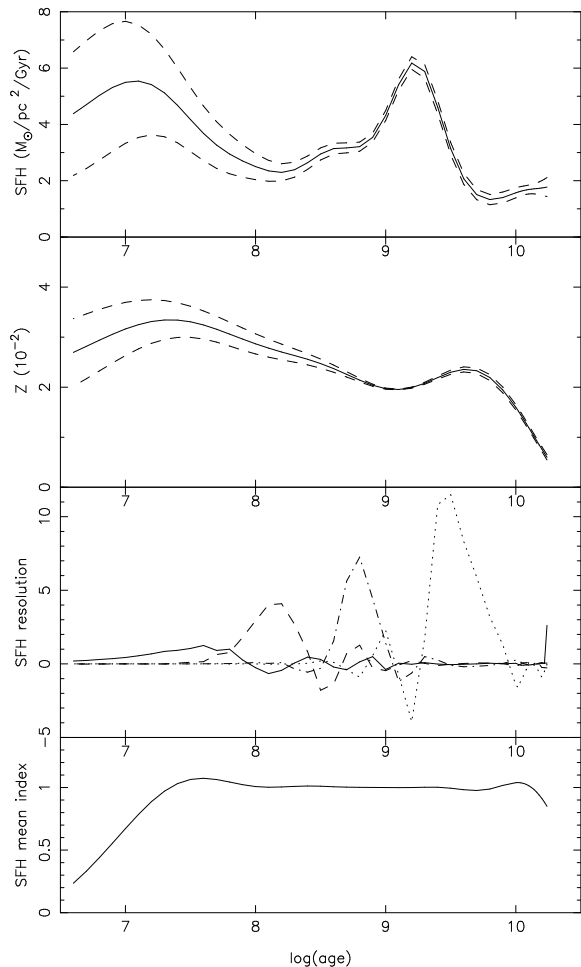
Fig. 6. The star formation history of the solar neighbourhood, assuming a constant stellar metallicity $Z = Z_\odot$. From top to bottom: The derived SFH with standard errors, the resolving kernel $K(t, t')$ as a function of age t for $\log(t') = 7.3, 8.1, 8.8$, and 9.6 (full, dashes, dot-dashes, and dots) and the mean index.

Fig. 7. Similar to Fig.7, but for the simultaneous inversion for SFH and AMR. The second panel from the top shows the deduced AMR with standard errors

Hernandez et al. (2000) use an inverse method to derive the SFH over the last 3 Gyr. They show clearly a bump in the SFH at about 2 Gyr. Similar to their results we do not find the decreasing SFH activity between 1 and 2 Gyr as found by Rocha-Pinto (1999) from chromospheric activity.

The determinations of the IMF (cf. Scalo 1986) yield that the present SFR should be nearly equal to the past average SFR. Our study gives the same result:

$$\frac{\int_0^{10\text{Gyr}} \psi(t)dt/10\text{Gyr}}{\psi(0)} = 0.9.$$

A quite different approach can be obtained from the chemical evolution of the solar neighbourhood: Rocha-Pinto & Maciel (1997) derived from the metallicity distribution of the G-dwarfs and the AMR the SFH (cf. Eqn. 13 below) taking into account the observational scatter. They demonstrate that for several observed AMRs one arrives at rather similar SFHs: a broad peak at about 8 Gyrs ago with about twice the present SFH and an epoch of low SFH (one half or less of the present value) between 1 and 3 Gyrs ago. As this approach requires the *slope* of the already rather uncertain and noisy AMR, the results are quite sensitive to the adopted AMR, e.g. the mean AMR of Edvardsson et al. (1993) gives a nearly flat SFH. At an age of 1.5 Gyrs, when the Hipparcos CMD gives a peak SFH, Rocha-Pinto & Maciel rather find a minimum. Though their result seems statistically significant, one should emphasize that this approach can yield only a resolution which is nearly constant in (linear) time, because the metallicity changes nearly linearly in time with some flattening near the present. On the contrary, the distribution of stars in a CMD is sensitive to the logarithm of the age. Therefore we feel that the Hipparcos CMD gives a stronger constraint on the SFH in the past few Gyrs. Certainly, this discrepancy between chemical evolution and stellar population needs further attention.

As a further check we investigate whether our SFH is in agreement with the past gas consumption in the solar
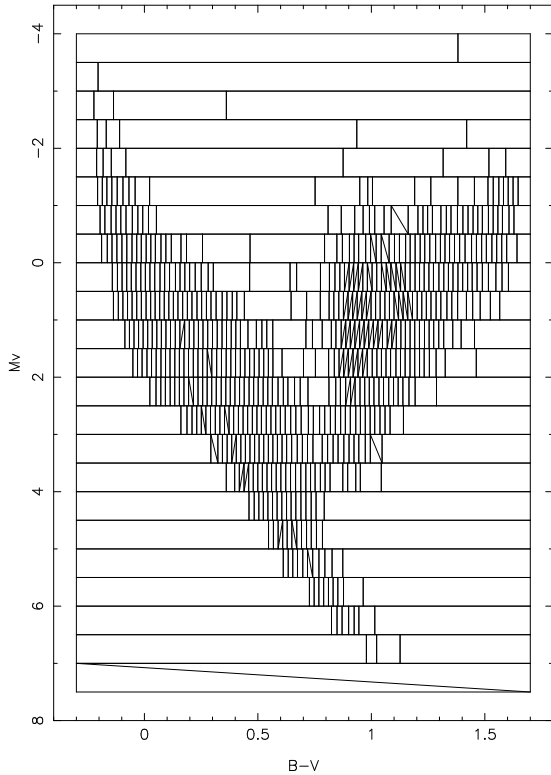
Fig. 8. Comparison of model and observed CMD: The / (\) indicate the bins whose number of model stars is smaller (greater) by at least 3σ than the observations
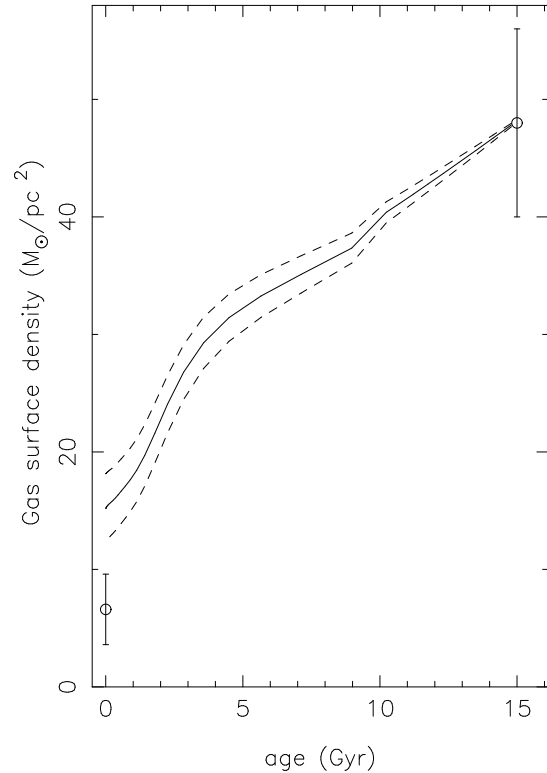

Fig. 9. Evolution of the gas surface density in the solar neighbourhood, computed with our SFH (solid line). The two dotted lines indicate the error at the $\pm 1\sigma$ level. The circle at 0 Gyr is the present surface gas density (Rana, 1992). The circle at 15 Gyr is the present dynamical density (Kuijken & Gilmore, 1991). For both values 1 σ error bars are given

neighbourhood: in a closed-box model the evolution of the surface gas density Σ_g is given by (Tinsley, 1980) :

$$\frac{d\Sigma_g}{dt} = -(1 - R)\psi(t). \tag{12}$$

The constant $(1-R)$ is the locked-up mass fraction, which is about 0.8 for a Salpeter IMF, and rather insensitive to the IMF. The total surface density of the mass present in the disk was derived from stellar dynamics by Kuijken & Gilmore (1991) as 48 $M_\odot \mathrm{pc}^{-2}$. The current gas surface density is 6.6 $M_\odot \mathrm{pc}^{-2}$ estimated by Rana (1992) as the sum of molecular and atomic hydrogen. Wyse & Gilmore (1995) argue for a somewhat higher present day gas fraction of 25 percent. Using the total mass as the initial condition, we integrate Eqn. 12. The evolution of the gas density shown in Fig. 9 matches the present day gas fraction rather well.
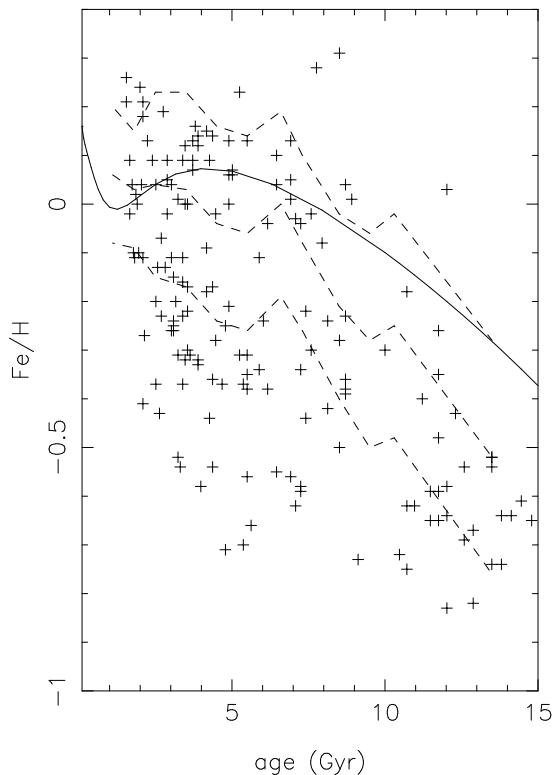
7.4.2. The age-metallicity relation

In their preliminary study, Bertelli et al. (1997) emphasized that the colour extension of the horizontal branch clump as well as the width of the main sequence provide evidence for an extended range ($Z = 0.008...0.03$) of metallicities in the stellar population. This is corroborated by our study, in the sense that a much better fit is obtained, if one allows for a variation of the metallicity.

The derived relation between age and metallicity is compared in Fig. 10 with those obtained by others. The metallicity increases with time, reaching a peak (at solar metallicity) at an age of 4 Gyr; thereafter it descends somewhat, going through a minimum at 1 Gyr, and then rising again. Though Fig. 7 shows that this wavy structure is significant, we prefer not to place too strong an emphasis on it, because on one hand the information is used for both SFH and AMR, that are treated as independent functions. With this greater amount of freedom, a good fit may well be achieved. On the other hand, the finding that the peak SFH at an age of 1.5 Gyr is not associated with or closely followed by a strong increase in the metallicity, as would be expected from chemical evolution, points well in the same direction. Also, the time resolution in the SFH is rather coarse (perhaps 0.3 dex) which also pertains to the AMR.

The causal link betwen star formation and metal enrichment could and should be used as a constraint to make the SFH and AMR consistent with each other. While it is conceivable that it be incorporated in our method, it is not the aim of the present paper to do that.

Fig. 10. Age-metallicity relations obtained with the inversion (full line) in comparison with the relation of Meusinger et al. (1991) – dashed lines giving the average and $\pm 1\sigma$ curves – Crosses are individual stars from Edvardsson et al. (1993).

Fig. 11. Metallicity distribution function for the G dwarfs (Rocha-Pinto & Maciel, 1997, dashed line) and computed from our SFH and AMR (full line)
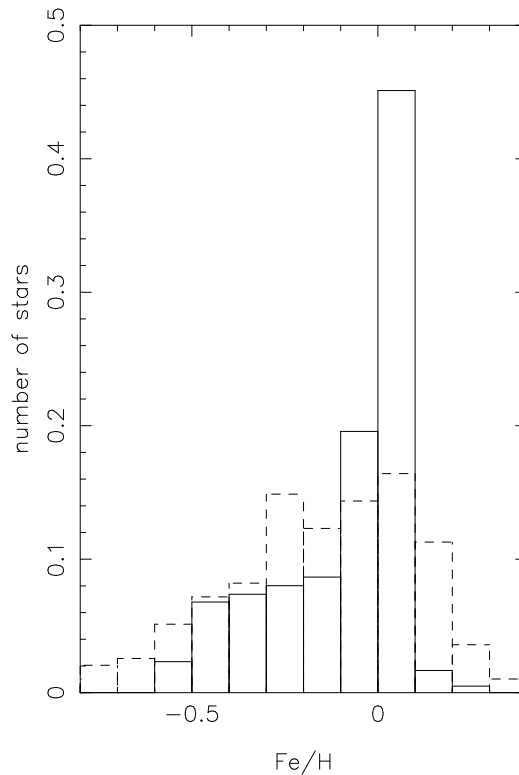
The histogram of the metallicities of the G dwarfs is a powerful constraint for the chemical evolution of the disk (cf. Pagel, 1997). From our SFH and the time derivative of our AMR we compute this distribution function as

$$dN_*/d\lg Z = \frac{dN_*/dt}{d\lg Z/dt} \propto Z \cdot \psi(t(Z))/(dZ/dt) \qquad (13)$$

which is shown in Fig. 11 in comparison to the histogram from Rocha-Pinto & Maciel (1997). Note that the distribution from Rocha-Pinto & Maciel suffers from the additional dispersion inherent to the measurements, that we did not try to simulate. Our distribution has a sharp peak near solar metallicity, because our AMR is rather flat at an age around 1 Gyr. This could be due to errors in the metallicities as determined with Strömgren photometry. Using their sample of G dwarfs, Rana & Basu (1990) show that the intrinsic dispersion of metallicity reaches 0.24 ± 0.10 dex at a given age.

8. Conclusions

The method presented here permits us to extract SFH, IMF slope and age-metallicity relations in a coherent way taking into account the selection function in apparent magnitude and the dispersion velocity of the stars. Indicators like the mean index and the resolution give a

good idea of the quality of the results. It shows clearly that the mixed populations cannot be separated with an infinite accuracy and that the results depends on the accuracy of the evolutionary tracks.

The observed Hipparcos HR diagram is well reproduced by the model at the main sequence level while the horizontal giant branch is not correctly fit. This could be due to the poor knowledge of the parameters that constrain the evolution of old stars. Also, our results could be biased by the presence of undetected binary stars or peculiar colour behaviour of A stars in the main sequence.

The derived SFH shows enhanced star formation about 1 to 2 Gyrs ago, while the present SFR is about equal to the past average SFR. This agrees well with the overall gas consumption in the solar neighbourhood. The AMR displays a systematic rise in metallicity with time. Both the AMR and SFH are fairly consistent with the paucity of metal-poor G dwarfs.

The principal result found in this study is that the thin disk of the Milky Way is rather young and has a solar metallicity.

References

Backus G., Gilbert F.: 1970, Phil. Trans. R. Soc. London 266, 123

Bertelli G., Bressan A., Chiosi C., Fagotto F., Nasi E.: 1994, A&AS 106, 275

Bertelli G., Nasi E., Bressan A., Chiosi C.: 1997, ESA SP-402, 501

Bertelli G. and Nasi E.: 2000, ApJ in press (astro-ph/0011126)

Craig I.J.D., Brown J.C.: 1986, *Inverse Problems in Astronomy*, Adam Hilger Ltd., Bristol and Boston

Crézé M., Chereul E., Bienaymé O., Pichon C.: 1998, A&A 329, 920

Dolphin A.: 1997, New Astronomy 2, 397

Dolphin A.: 2001, MNRAS in press (astro-ph/0112331)

Edvardsson B., Andersen J., Gustafsson B., Lambert D.L., Nissen P.E., Tomkin J.: 1993, A&A 275, 101

ESA: 1997, *The Hipparcos and Tycho Catalogues, Volume 1*, SP-1200, 131

Flynn C., Fuchs B.: 1994, MNRAS 270, 471

Gallart C., Aparicio A., Bertelli G., Chiosi C.: 1996, AJ 112, 1950

Girardi L., Bressan A., Bertelli G., Chiosi C.: 2000, A&AS 141, 371

Gómez A.E., Grenier S., Udry S., Haywood M., Meillon L., Sabas V., Sellier A., Morin D.: 1997, ESA SP-402, 621

Greggio L., Marconi G., Tosi M., Forcadi P.: 1993, AJ 105, 894

Harris J., Zaritsky D.: 2001, ApJS 136, 25

Haywood M., Robin A., Crézé M.: 1997, A&A 320, 428

Hernandez X., Valls-Gabaud D., Gilmore G.: 1999, MNRAS 304, 705

Hernandez X., Valls-Gabaud D., Gilmore G.: 2000, MNRAS 316, 605

Holmberg J., Flynn C.: 2000, MNRAS 313, 209

Köppen J.: 1994, A&A 281, 26

Kroupa P., Tout C.A., Gilmore G.: 1993, MNRAS 262, 545

Kuijken K., Gilmore G.: 1991, ApJ 367, L9

Kuijken K., Gilmore G.: 1989, MNRAS, 239, 605

Meusinger H., Reimann H.G., Stecklum B.: 1991, A&A 245, 57

Meyer D.M., Jura M.J., Hawkins I., Cardelli J.A.: 1994, ApJ 437, L59

Ng Y.K., Bertelli G.: 1998, A&A 329, 943

Perryman M.A.C. et al.: 1997, A&A 323, L49

Pagel B.E.J.: 1997, "Nucleosynthesis and Chemical Evolution of Galaxies", Cambridge University Press

Rana N.C., Basu S.: 1990, Ap&SS 168, 317

Robin A.C., Haywood M., Crézé M., Ojha D. K., Bienaymé O.: 1996, A&A 305, 125

Rocha-Pinto H.J., Maciel W.J.: 1997, MNRAS 289, 882

Rocha-Pinto H.J., Scalo J., Maciel W.J., Flynn C.: 2000a, ApJ 531, L115

Rocha-Pinto H.J., Maciel W.J., Scalo J., Flynn C.: 2000b, A&A (astro-ph/0001382)

Salpeter E.E.: 1955, ApJ 121, 161

Saporta G.: 1990, *Probabilités*, Editions Technip, Paris

Scalo J.M.: 1986, Fund. Cosmic Phys. 11, 1

Tarantola A., Valette B.: 1982a, J.Geophys. 50, 159

Tarantola A., Valette B.: 1982b, Rev. Geophys.& Space Phys. 20, 219

Tinsley B.M. : 1980, Fund. Cosmic Phys. 5, 287

Tolstoy E., Saha A.: 1996, ApJ 462, 672

Twomey S.: 1977, "Introduction to the Mathematics of Inversion in Remote Sensing and Indirect Measurements", Dover, New York

Vergely J.-L.: 1998, Ph.D. Thesis, Obs. de Strasbourg

Wielen R.: 1977, A&A 60, 263

Wyse R.F.G, Gilmore G., 1995, AJ 110, 2771